Available online at www.sciencedirect.com
SCIENCE DIRECT
Journal of Catalysis 227 (2004) 398–407
JOURNAL OF CATALYSIS
www.elsevier.com/locate/jcat

$(NH_4)_2SiF_6$-modified ZSM-5 as catalysts for direct hydroxylation of benzene with N_2O 1. Influence of the treatment method

Felix Kollmer, Heike Hausmann, Wolfgang F. Hölderich *

Department of Chemical Technology, University of Technology RWTH Aachen, Worringerweg 1, 52074 Aachen, Germany

Received 10 February 2004; revised 24 June 2004; accepted 1 July 2004

Available online 3 September 2004

Abstract

Two samples of MFI-type zeolites (A, $SiO_2/Al_2O_3 = 30$, 0.02 wt% Fe, and B, $SiO_2/Al_2O_3 = 20$, 0.03 wt% Fe) were dealuminated with $(NH_4)_2SiF_6$ by three different methods. Method (i) consisted of aqueous treatment in a buffered solution followed by thorough washing with distilled water. Method (ii) consisted of isomorphous substitution in the solid state at moderate temperatures followed by thorough washing with deionized water. Method (iii) involved the removal of aluminum fluoro complexes by thermal decomposition after the preceding solid-state isomorphous substitution procedure. The materials were characterized by ICP-AES, physisorption of N_2, XRD, FT-IR, PyFT-IR, and ^1H, ^{27}Al, ^{29}Si, and ^{19}F MAS NMR prior to and after catalytic testing for direct hydroxylation of benzene to phenol. It was shown that the materials were loaded with considerable amounts of F^- in the form of Al–F and Si–F prior to the reaction, which disappeared quantitatively after the reaction. Catalytic properties, in terms of activity and the rate of deactivation, could be correlated to acid–base and textural properties. Materials prepared according to method (iii) showed the best catalytic activity. Materials prepared according to method (ii) showed moderate activity, whereas the formation of phenol was hardly detected over materials prepared according to method (i).

Keywords: Dealuminated ZSM-5; $(NH_4)_2SiF_6$; Lewis acidity; Phenol; Pyridine adsorption; FT-IR; Solid-state dealumination; Deactivation; Coking

1. Introduction

Direct synthesis of phenol from benzene and nitrous oxide has attracted considerable attention because of its potential economic advantage and eco-efficiency compared to the widely used cumene process.

Pentasil zeolites have been identified as a promising class of catalysts [1–3]. Concerning the active site two main directions are followed nowadays, because the concept of Brønsted acid hydroxyls dating back to the early days [1,4] has not been followed recently [5]. The research group of the Boreskov Institute of Catalysis promotes the idea of the exclusive catalytic activity of iron species [6,7], the so-called α-sites. The reaction is thought to proceed via a surface oxygen species formed upon stoichiometric decomposition of N_2O. The assumption that iron is the sole active compound has been investigated by a number of other research groups, though sometimes with different ideas on the structure and stoichiometry of the active site. Some groups agree with Panov's ideas about dinuclear oxobridged Fe species [8,9], while others consider that isolated Fe ions [10] are responsible. Hensen et al. identified Fe^{2+} species as α-sites for nitrous oxide decomposition [11]. Other researchers extended the idea of coordinatively unsaturated Lewis acidic framework [12] or nonframework [13] sites that are not related to the presence of iron. Kustov et al. [12] postulated exclusive catalytic activity by framework defects which formed upon dehydroxylation of bridging Si(OH)Al sites. The concept of Lewis acid aluminum species as active sites was widened by Motz et al. [13,14] via mild hydrothermal treatment of ZSM-5 zeolites, thus intentionally creating extraframework

* Corresponding author. Fax: +49(0)241 802 22 91.
E-mail address: hoelderich@rwth-aachen.de (W.F. Hölderich).

0021-9517/$ – see front matter
doi:10.1016/j.jcat.2004.07.008

aluminum (EFAL). Recently Hensen et al. brought together those models and showed the necessity of both aluminum and iron, thus postulating Al–O–Fe moieties as active sites [11]. Many research groups observed more or less rapid deactivation due to coke formation, which might be a serious obstacle to commercializing the process. Most of them assume that Brønsted sites are a key factor in coke formation by catalyzing consecutive reactions of phenol [5,12,15]. Ivanov et al. [16], however, suggested that coke formation happens exclusively on the α-sites, and that diffusion hindrance, due to pore clogging, is not a decisive factor.

Dealumination by treatment with fluorinous reagents has been known for a long time. It is an effective and, in the case of $(NH_4)_2SiF_6$, an industrial method for increasing the framework Si/Al ratio (e.g., [17,18]). However, despite the numerous reports on modified zeolites for the benzene-to-phenol reaction, to the best of our knowledge this treatment has not been studied in detail. Thus a comparative study, in which the preparation method and the SiF_6^{2-}/framework aluminum (FAL) ratio were varied, was conducted. The procedure was carried out (i) in a buffered aqueous solution similar to the method of Skeels et al. [19], (ii) in the solid state with subsequent washing with distilled H_2O [20,21], and (iii) in the solid state followed by thermal decomposition of AlF_6^{3-} species formed during isomorphous substitution. The degree of dealumination is expected to be controlled by the amount of $(NH_4)_2SiF_6$ per amount of zeolite. In addition some of the modified samples were also subjected to steam treatment in order to assess the long-term stability for potential practical applications.

2. Experimental

2.1. Catalysts

HZSM-5 zeolite (KAZ 93/77-79 KM1415) was kindly provided by Degussa AG, Hanau. It was dried for 2 h at 150 °C and calcined for 12 h at 550 °C (3 °C/min). Subsequently the material was washed three times with diluted HCl (6 h, 70 °C, $c_{HCl} = 0.001$ mol/L, 10 ml/g). The zeolite was transferred to the NH_4^+ form by a threefold ion exchange in aqueous NH_4NO_3 (70 °C, 3 h, 1 M NH_4NO_3, 10 ml/g zeolite) and was subsequently dried in air at 150 °C for 18 h. The hydrogen form was obtained by calcination in air at 550 °C for 6 h and was the basis material for further modification (A-550) ($SiO_2/Al_2O_3 = 30$, $Na/Al < 0.02$, 0.02 wt% Fe_2O_3).

TPABr (44.4 g), NaOH (22.7 g), $NaAl_2O$ (11.8 g), and 100 g SiO_2 (aerosil) were dissolved in 1080 g H_2O and stirred for 18 h. The resulting gel was transferred to Teflon-lined autoclaves, where hydrothermal synthesis under autogeneous pressure took place at 150 °C during 5 days. The solid was recovered by filtration, thoroughly washed with deionized water, dried at 150 °C for 18 h, and calcined in air in a shallow bed for 24 h at 550 °C. The zeolite was transferred to the NH_4^+ form by a threefold ion exchange in aqueous NH_4NO_3 (70 °C, 3 h, 1 M NH_4NO_3, 10 ml/g zeolite) and was subsequently dried in air at 150 °C for 18 h. The hydrogen form was obtained by calcination in air at 550 °C for 6 h and was the basis material for further modification (B-550) ($SiO_2/Al_2O_3 = 20$, $Na/Al = 0.04$, 0.03 wt% Fe_2O_3). Both basis materials showed the typical MFI diffractions in XRD, and ^{27}Al NMR revealed the visible Al in tetrahedral coordination.

For dealumination according to method (i) zeolite powder was stirred in a glass reactor, placed in an oil bath, and equipped with a reflux unit, with an aqueous solution of $(NH_4)_2SiF_6$ and CH_3COONH_4. The treatment temperature was usually 75 °C and 10 ml solution per gram of solid was applied. A stoichiometric amount of $(NH_4)_2SiF_6$ with respect to FAL was added and the time of the treatment was 21 h. The solid was recovered by filtration, thoroughly washed with hot deionized water, and dried for 18 h at 150 °C (A-SiF6-100aq). For dealumination according to method (ii) zeolite powder was closely mixed in an agetate mortar with an appropriate amount of $(NH_4)_2SiF_6$ to ensure complete replacement of FAL. The mixture was placed in a desiccator over $NH_{3\,aq}$ for 18 h, then placed in a quartz tube ($d_i = 40$ mm) and kept at 160 °C for 48 h in a constant flow of dry N_2. After the solid-state reaction the solid was thoroughly washed with hot deionized water and dried for 18 h at 150 °C (A-SiF6-100S-aq). For method (iii) zeolite powder was intimately mixed in an agetate mortar with an appropriate amount of $(NH_4)_2SiF_6$ to ensure the desired degree of replacement of FAL. The mixture was placed in an desiccator over $NH_{3\,aq}$ for 18 h, then placed in a quartz tube ($d_i = 40$ mm), kept at 160 °C for 48 h, and subsequently heated to 550 °C for 6 h. The treatment took place in a steady flow of dry N_2. The samples were labeled with A-SiF6-*n*S and B-SiF6-*n*S, where *n* is the percentage ratio of SiF_6^{2-}/FAL.

The samples A-SiF6-100S and B-SiF6-100S were subsequently subjected to a hydrothermal treatment at 550 °C and 500 mbar H_2O partial pressure for 3 and 6 h, respectively (A-SiF6-100S-st3 and B-SiF6-100S-st6).

2.2. Characterization

X-ray powder diffractograms (not shown) were collected on a Siemens D-5000, equipped with a secondary monochromator, a variable diaphragm V 20, and a nickel filter with Cu-K_α radiation. The elemental composition was determined by ICP-AES (Spectroflame D, Spectro) after digestion in a mixture of dilute HF and H_2SO_4. The crystallite size distribution has been kindly provided by Beckmann–Coulter GmbH, Krefeld, using a Coulter counter. Both basis materials showed a narrow Gaussian-shaped distribution with a maximum at 3.3 μm for sample A-550 and 5.4 μm for sample B-550. The IR spectra were recorded on a Nicolet Protegé 460 with a resolution of 0.25 cm^{-1} for estimation of framework vibrations and 2 cm^{-1} for hydroxyl vibrations

and the use of pyridine as probe. To investigate hydroxyl vibrations and interactions of pyridine the materials have been fabricated to self-supporting wafers and placed in a home-made IR cell. Prior to measurement the wafer was outgassed for 18 h at 400 °C and 10^{-1} Pa (2 °C/min heating rate) and subsequently cooled to 150 °C, where the spectrum was taken. Band areas of chemisorbed pyridine on Brønsted (1550 cm^{-1}) and Lewis acid (1450 cm^{-1}) sites have been referred to the band area of structural vibrations at 1870 and 1981 cm^{-1}, which represent the quantity of zeolite exposed to radiation.

Physisorption of N_2 at 77 K was carried out on a volumetric apparatus (ASAP 2010, Micromeritics) in a static mode. The samples were evacuated prior to measurement at 400 °C and 10^{-2} Pa for 18 h. Microporosity was calculated according to the method of Dubinin [22] and compared to the uptake at $p/p_0 = 0.05$. Mesoporosity was computed according to the method of Barrett, Joyner, and Halenda (BJH) [23] and compared to the difference between the total uptake and the microporous volume. The agreement between the alternative methods was satisfactory in all cases.

^{1}H, ^{27}Al, and ^{29}Si NMR spectra were recorded on a Bruker DSX 500 spectrometer. The resonance frequencies were ^{1}H, 500.46 MHz; ^{27}Al, 130.41 MHz; and ^{29}Si, 99.43 MHz. ^{29}Si MAS spectra were taken using 7-mm double-bearing MAS NMR probes and a sample rotational speed of 5 kHz. For the ^{1}H MAS spectra a 4-mm probehead and a spinning rate of 12 kHz were used. Magic-angle spinning (MAS) with a rotational speed of 5 kHz was applied for all the ^{27}Al spectra recorded with a 7-mm probehead and with a rotational speed of 20 kHz for all the ^{27}Al spectra recorded with a 2.5-mm probehead. The ^{1}H and ^{29}Si NMR spectra were referenced with respect to external TMS. All the ^{27}Al chemical shifts were referred to external $[Al(H_2O)_6]^{3+}$ in $Al(NO_3)_3 \cdot H_2O$. Prior to the ^{27}Al NMR measurements, the zeolite samples were equilibrated with H_2O for 18 h. Prior to the ^{1}H NMR measurements, physisorbed H_2O was removed at 400 °C (1 °C/min) and 10^{-2} Pa. The ^{19}F MAS NMR measurements were carried out on a Bruker MSL 300 spectrometer at a resonance frequency of 282.2 MHz using 4 mm MAS NMR probes and at a sample spinning rate of 3–10 kHz. The ^{19}F NMR shifts were referenced to an external standard of C_6F_6 (−163 ppm CF_3Cl).

2.3. Catalytic tests

The catalyst was pressed into tablets, crushed, and sieved. The amount of 1.5 g of dry zeolite with a particle size fraction of 250–500 µm was subjected to catalytic tests performed in a vertical tubular plug flow reactor (d_i = 8 mm). Gaseous reactants were fed by thermal mass-flow controllers. Benzene was fed by a laboratory-scale piston pump into a capillary evaporator. N_2O (medical grade purity) was obtained by Air Liquide, and benzene was supplied by Fluka (> 99.5%). Modified residence time W/F was 20 (kg_{cat} s)/mol and the composition of the feed mixture was $C_6H_6/N_2O/N_2 = 4/2/1$ on a molar basis. Bodenstein's number was calculated to values of 200–300; i.e., plug flow can be assumed. The reaction products were sampled in regular time scales in a cooling trap and analyzed by GC (HP6890, 30 m FT-SE54 column). The mass balance was obeyed within ±5% and the selectivity of phenol referred to benzene exceeded in all cases 95%. The absence of significant deep oxidation was qualitatively checked by absorption of the off-gas stream in a scrubber filled with an aqueous $Ca(OH)_2$ solution. Prior to reaction the catalysts were conditioned at 500 °C for 1 h in a steady flow of N_2/N_2O and subsequently cooled to 350 °C. Activity and rate of deactivation were evaluated by a method proposed by Levenspiel [24]. Assuming first-order deactivation and a gradientless reactor, e.g., differential conversion, i.e., proportionality of reaction rate $r(t)$ and conversion $X(t)$,

$$\mathrm{d}a(\mathrm{TOS})/\mathrm{dTOS} = k_\mathrm{d} a(\mathrm{TOS}) \Leftrightarrow a(\mathrm{TOS}) = \exp[-k_\mathrm{d}\mathrm{TOS}], \quad (1)$$

the dependence of the conversion on time on stream TOS can be written as

$$X(\mathrm{TOS}) = X_0 \exp[-k_\mathrm{d}\mathrm{TOS}], \quad (2)$$

with k_d as characteristic time constant of deactivation, that is, correlated with the half-live period $t_{0.5}$:

$$t_{0.5} = \ln 2/k_\mathrm{d}. \quad (3)$$

Thus, a semilogarithmic plot of conversion of benzene vs time on stream yields a straight line with the initial conversion X_0 as the intercept and the rate constant of deactivation k_d as negative slope.

3. Results and discussion

3.1. Characterization

Data on the elemental composition and the state of aluminum of modified materials before and after catalytic testing are disclosed in Table 1. For materials prepared according to methods (ii) and (iii) the aluminum content determined by ICP-AES before catalytic tests is considerably lower than after use. The deviation seems to depend on the amount of $(NH_4)_2SiF_6$ added and is more pronounced for method (iii). This phenomenon is ascribed to the limited solubility of AlF_3, formed during the solid-state isomorphous substitution (vide infra). After reaction and hydrothermal treatment, aluminum levels on materials modified with method (iii) are as expected in close vicinity to those of the basis material, since there are few reports in the literature on volatile aluminum species. Comparing methods (i) and (ii), both comprising a liquid extraction, method (ii) leads to a far more effective reduction of the bulk Si/Al ratio. This indicates a more effective replacement of FAL in the solid state

Table 1
Properties of $(NH_4)_2SiF_6$-treated materials

	Before modification	Before use		After use		
	Al[a] (u.c.)	Al[a] (u.c.)	Al_{th}[b] (u.c.)	Al[a] (u.c.)	Al_{th}[b] (u.c.)	$\Delta\nu$[c] (cm^{-1})
A-550	6.4	6.4	6.4	6.4	n.d.	0
Method (i)						
A-SiF6-100aq	6.0[d]	6.0[e]	6.5	5.8	5.8	−2.7
Method (ii)						
A-SiF6-100S-aq	6.0[f]	2.3	3.7	4.0	3.0	4.4
Method (iii)						
A-SiF6-20S	6.3[f]	6.3	4.7	6.3	3.6	3.8
A-SiF6-40S	6.3[f]	4.2	1.7	6.3	2.0	7.1
A-SiF6-60S	6.2[f]	2.6	0.5	6.3	1.7	7.5
A-SiF6-100S	6.0[f]	2.2	< 0.5	6.3	1.5	8.7
Method (iii) + steam						
A-SiF6-100S-st3	n.d.	n.d.	n.d.	n.d.	2.2	7.9
B-550	9.6	9.6	9.6	9.6	n.d.	0
Method (iii)						
B-SiF6-100S	9.2	8.2	< 0.5	9	3.6	8.8
Method (iii) + steam						
B-SiF6-100S-st6	n.d.	n.d.	n.d.	9	3.8	9.3

[a] Determined by ICP-AES.
[b] Tetrahedral aluminum determined by ^{27}Al NMR.
[c] Shift of the band maximum of the asymmetric T–O–T stretching vibration at ∼ 1100 cm^{-1} in FT-IR.
[d] Overall composition of the solid and $(NH_4)_2SiF_{6\ aq}$ added (calculated).
[e] Composition of the dry solid.
[f] Composition of the mechanical mixture of A-550 and $(NH_4)_2SiF_6$.

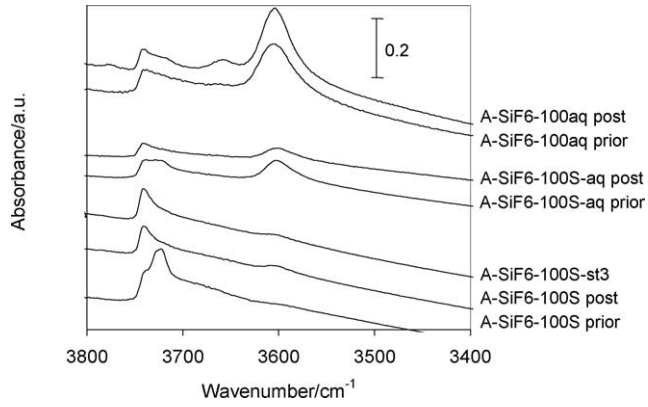

Fig. 1. FT-IR spectra of the hydroxyl region of $(NH_4)_2SiF_6$-modified samples according to methods (i)–(iii) prior to and after catalytic tests. Samples derived from basis material A.

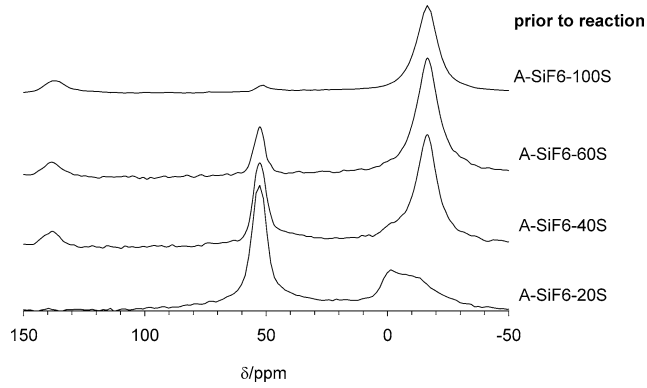

Fig. 2. ^{27}Al MAS NMR spectra of samples treated with $(NH_4)_2SiF_6$, according to method (iii) prior to catalytic testing. Samples derived from basis material A.

at elevated temperatures compared to the liquid-phase procedure. This fact is also reflected in the content of tetrahedral aluminum measured by ^{27}Al NMR, the shift of asymmetric T–O–T vibration in the FT-IR spectra (Table 1), and the difference in mesoporous volumes (see Table 3).

Besides a well-resolved peak at 55 ppm due to tetrahedral aluminum the ^{27}Al MAS NMR spectra (not shown) of both materials prior to reaction contain a broad peak at 0 ppm, more pronounced after treatment with method (ii) due to distorted octahedrally coordinated aluminum species. After the reaction a relatively sharp peak at 0 ppm due to dealumination under reaction/regeneration conditions can be observed in the spectrum of sample A-SiF6-100aq analogous to the one in the basis material A-550. This effect is less pronounced on sample A-SiF6-100S-aq, possibly due to the lower aluminum content and, therefore, enhanced hydrothermal stability.

Hydroxyl groups associated with EFAL, causing a band at 3665 cm^{-1} [25,26] in the FT-IR spectrum, vanish after treatment with $(NH_4)_2SiF_6$ regardless of the method (Fig. 1). This is due either to their replacement with F^- or to the removal of EFAL by the aqueous extraction procedures of methods (i) and (ii). After the reaction and after the steam treatment they are abundant only on sample A-SiF6-100aq, consistent with the results of ^{27}Al MAS NMR of samples treated with methods (i) and (ii). After dealumination in the solid state (methods (ii) and (iii)) also a distinct peak at 3720 cm^{-1} in the FT-IR spectra can be observed. This band is assigned by internal silanol groups, most possibly on lattice defects [25], hydroxyl groups on extrazeolitic material [27], or terminal silanol groups whose acidic strength is enhanced by interaction with EFAL [28]. Two bands due to SiOH groups are also observed in the ^{1}H NMR spectrum of A-SiF6-100S prior to reaction (Fig. 5). The facts that these bands vanish after reaction/regeneration and hydrothermal treatment and are more pronounced for more rigorous dealumination with method (iii) (see Table 1 and below) and that the infrared band hardly interacts with pyridine (not shown) suggest that we are indeed dealing with silanol groups on structural defects caused by the incomplete substitution of FAL during the solid-state reaction.

Method (iii) is the most effective of the three for reducing tetrahedral aluminum and creating octahedral aluminum as it is visualized in Fig. 2 and in Table 1. This is most probably due to the evolution of reactive substances, such as NH_4F, SiF_4, and HF, upon thermal decomposition of AlF_6^{3-} and nonreacted SiF_6^{2-}. Those chemicals can further react with the zeolite framework at higher temperatures. Two

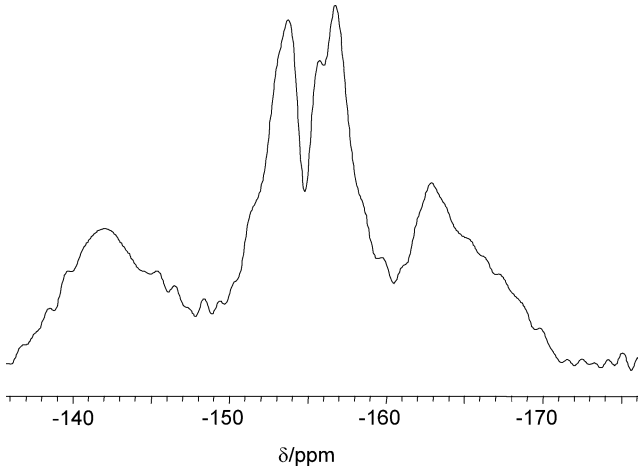

Fig. 3. ^{19}F MAS NMR spectra of $(NH_4)_2SiF_6$-treated samples (method (iii)) prior to reaction. Sample A-SiF6-100S. Chemical shift referred to CF_3Cl.

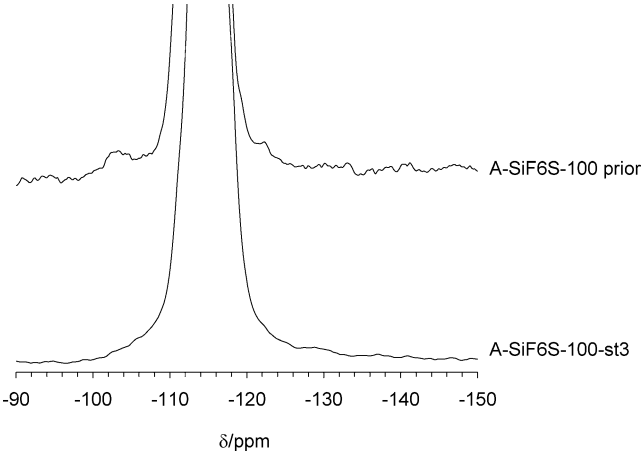

Fig. 4. ^{29}Si MAS NMR spectra of samples treated with $(NH_4)_2SiF_6$ according to method (iii) prior to reaction and after subsequent hydrothermal treatment. Samples derived from basis material A.

types of octahedral aluminum are found in samples examined prior to catalytic tests: aluminum (hydr)oxide species with a chemical shift δ_{Al} of 0 ppm, as frequently observed in (hydro)thermally treated samples, and aluminum fluoro species with a chemical shift δ_{Al} of −15 ppm, also observed in ZSM-5 samples treated with molecular fluorine [18]. As

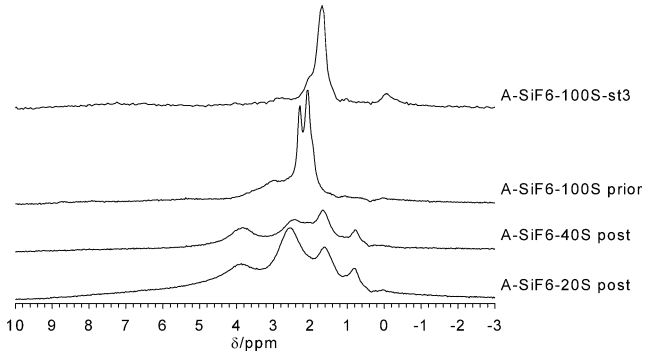

Fig. 5. ^{1}H MAS NMR of samples treated with $(NH_4)_2SiF_6$ according to method (iii) before and after catalytic testing and subsequent hydrothermal treatment.

the amount of added $(NH_4)_2SiF_6$ increases, the number of tetrahedral aluminum decreases. Complete removal of tetrahedral aluminum can be achieved for both basis materials in the case of stoichiometric amounts of Si in $(NH_4)_2SiF_6$ referred to FAL. Simultaneously also the fraction of fluorinated octahedral aluminum increases sharply. In samples A-SiF6-100S and B-SiF6-100S the NMR visible aluminum is completely fluorinated (Fig. 2). The formation of Si–F species is evidenced by a peak at −103 ppm in the ^{29}Si MAS NMR spectrum of sample A-SiF6-100S (Fig. 4) [29]. The peaks in ^{1}H NMR spectra due to SiOH and AlOH on EFAL are also shifted to a lower field (Fig. 5) prior to reaction. These observations are consistent with a deshielding effect of the ^{1}H nuclei [30] due to the electron-withdrawing forces of F^- in the vicinity, as has been proposed by Le Van Mao et al. [31] and Borade et al. [32] in the case of NH_4F-impregnated zeolite samples (Fig. 6).

The formation of Si–F and octahedral aluminum fluoro species is also corroborated by ^{19}F NMR (Fig. 3). ^{19}F NMR spectra of HZSM-5, dealuminated according to method (iii), are looking very similar to the ones treated with molecular F_2 at RT (Fig. 5 in Ref. [18]). According to Sánchez et al. [18], the broad band at around −141 ppm and the shoulder at around −152 ppm can be assigned to fluorine bonded to silicon, whereas the lines at −155, 157, 158, and 165 ppm can be attributed to fluorine bonded to cationic octahedrally coordinated fluoro (hydr)oxide aluminum complexes. The

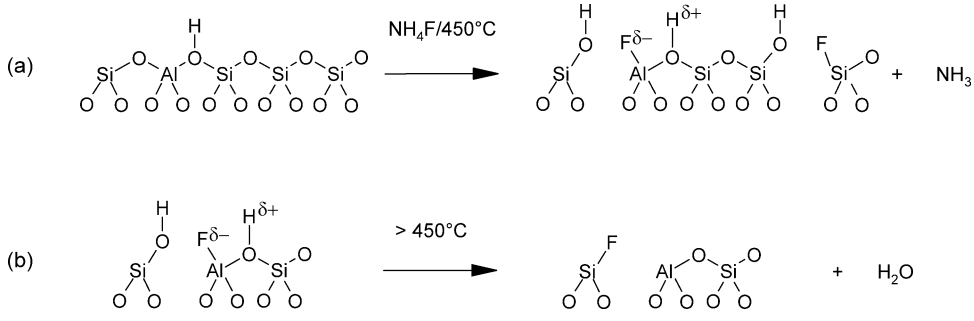

Fig. 6. Possible interaction of fluoride with the zeolite framework (adapted from [31,32]). (a) Enhancement of BA and formation of silanols, (b) removal of BA due to higher temperatures and higher F^- loading.

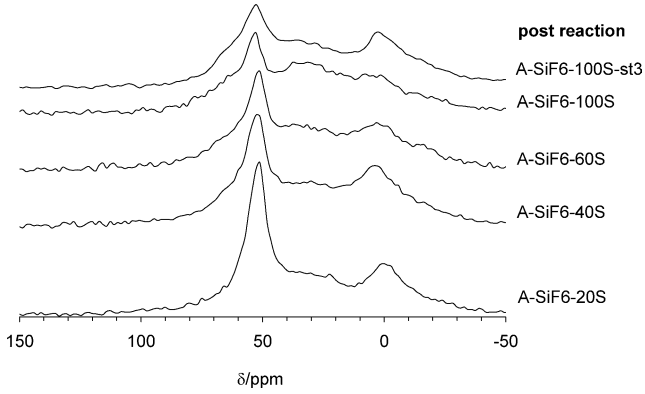

Fig. 7. ^{27}Al MAS NMR spectra of samples treated with $(NH_4)_2SiF_6$ according to method (iii) after reaction and after subsequent steam treatment. Samples derived from basis material A.

multiciplity of lines is assigned to the variable stoichiometry of those complexes.

The state of the aluminum, however, changes tremendously after exposure to humidity and elevated temperatures due either to reaction/regeneration conditions or to intentional hydrothermal treatment, as shown in Fig. 7.

Neither the Si–F species (Fig. 4) nor the aluminum fluoro species are now visible. Instead, a peak at 30 ppm appears in the ^{27}Al NMR spectra which is attributed by some research groups to penta-coordinated aluminum [33–36] and by others to distorted tetrahedral coordinated aluminum in EFAL [37–39] or distorted FAL, whose charge is compensated by cationic EFAL [40]. In the least dealuminated sample (A-SiF6-20S) the fraction of tetrahedral aluminum further decreases most possibly due to the release of F^- in the form of HF leading to hydrolysis of FAL. On the other hand, in deeply dealuminated samples (A-SiF6-40S, A-SiF6-60S, A-SiF6-100S, B-SiF6-100S) the amount of tetrahedral aluminum increases.

Several possible explanations exist for the return of the signal at 55 ppm after reaction/regeneration and hydrothermal treatment: (1) Tetrahedral aluminum is in such a distorted coordination sphere upon fluoridation that it is undetectable by NMR. (2) Aluminum is partially removed from the zeolite framework in an octahedral coordination, which is either invisible or causes peaks with a chemical shift of $\delta_{Al} = 015$ ppm (see, e.g., Fig. 6). Upon elevated temperature and humidity, defluoridation and reinsertion take place. (3) Tetrahedral EFAL is possibly in a separate amorphous silica/alumina phase. Possibility (1) cannot be ruled out completely, even though one rather expects octahedral aluminum with a distorted coordination sphere to be invisible to NMR [41]. Nevertheless, the fraction of NMR-visible aluminum in samples A-SiF6-100S and B-SiF6-100S, prior to catalytic tests and subsequent steaming, has been $\sim 60\%$ of the total aluminum; the fraction of tetrahedral aluminum in those samples after reaction and in the subsequently steamed ones A-SiF6-100S-st3 and B-SiF6-100S-st6 is 35–40% in each case.

With respect to (2), the existence of octahedral FAL [42–44] and its possible reinsertion upon impregnation with NH_4F and subsequent calcination [32] have been proposed by other authors. These reports refer, however, to β-zeolite only. Beyer et al. [20] and Han et al. [45] also reported that the isomorphous substitution procedure with fluoro species can be reversible under certain reaction conditions.

Furthermore the slight increase in the microporous volume (Table 3), the slight increase in the 3610 cm^{-1} band in FT-IR (Fig. 1), and the slight increase in the density of Brønsted acid sites (Table 2) upon catalytic testing and steaming are indicative of reinsertion of partially hydrolyzed aluminum. However, the shift in the T–O stretching vibration (Table 1) indicates strong framework dealumination and does not support the idea of a large extent of reinsertion. Also the levels of Brønsted-bonded pyridine (Table 2) rather correlate to the levels of tetrahedral aluminum prior to catalytic tests (Table 1) than the respective values for the samples after the catalytic tests and after subsequent steam treatment. This indicates that if tetrahedral aluminum is built in the zeolite lattice, it does not bear protons as charge compensation but probably bears instead cationic EFAL species. The pyridine adsorption data are supported by the FT-IR spectrum of hydroxyl groups (Fig. 1) and the ^{1}H MAS NMR spectrum of the subsequently steam-treated sample A-SiF6-100-st3 (Fig. 5), excluding that Brønsted acidic protons are present, but inaccessible to pyridine due to partial destruction of the zeolite lattice.

The formation of a separate noncrystalline phase with tetrahedrally coordinated aluminum (3) is also a realistic possibility. The N_2 physisorption isotherms of MFI-type materials can exhibit an additional hysteresis loop in the low pressure region ($0.1 < p/p_0 < 0.3$) [46], a range in which capillary condensation of N_2 does not occur [47]. In situ neutron diffraction measurements [48,49] revealed that the phenomen is due to phase transition of both the solid (monoclinic-orthorhombic) and the adsorbate (liquid–solid). This peculiar feature is related to a low FAL content; and the shape and the size of this hysteresis loop is even more pronounced with an increasing framework Si/FAL ratio and increasing size of the crystals. It can be safely assumed that the latter did not change during the modifications; thus, a change in the shape of the adsorption isotherms can be qualitatively interpreted as a consequence of framework dealumination.

Fig. 8 shows the low pressure range of N_2 adsorption isotherms of some of the samples treated according to method (iii) before and after reaction and after steam treatment. Indeed, the size of the hysteresis loop increases with increasing severity of the dealumination treatment and exposure to elevated temperatures and humidity. In the case of sample A-SiF6-40S it appears only after catalytic test reactions. Therefore, realumination during catalytic application or steaming occurs only to a minor extent. The main modification is further framework dealumination, possibly enhanced by HF formed by hydrolysis of the Al–F and Si–F species. It should be noted that in the present

Table 2
Acid–base properties of $(NH_4)_2SiF_6$-treated materials before and after catalytic tests

	Before use				After use			
	$A_{Br,\ spec.}$[a]	$A_{Le,\ spec.}$[b]	A_{Le}/A_{Br}	$(A_{Br}+A_{Le})_{spec.}$	$A_{Br,\ spec.}$[a]	$A_{Le,\ spec.}$[b]	A_{Le}/A_{Br}	$(A_{Br}+A_{Le})_{spec.}$
A-550	–	–	–	–	0.127	0.023	0.181	0.15
Method (i)								
A-SiF6-100aq	0.19	0.011	0.060	0.20	0.13	0.020	0.155	0.15
Method (ii)								
A-SiF6-100S-aq	0.054	0.006	0.104	0.06	0.053	0.006	0.107	0.06
Method (iii)								
A-SiF6-20S	n.d.	n.d.	n.d.	n.d.	0.064	0.018	0.278	0.08
A-SiF6-40S	n.d.	n.d.	n.d.	n.d.	0.031	0.022	0.713	0.05
A-SiF6-60S	0.017	0.007	0.417	0.02	0.018	0.013	0.693	0.03
A-SiF6-100S	0.006	0.005	0.776	0.01	0.011	0.007	0.582	0.02
Method(iii) + steam								
A-SiF6-100S-st3	–	–	–	–	0.004	0.006	1.38	0.01
B-550	–	–	–	–	0.10	0.033	0.336	0.13
Method (iii)								
B-SiF6-100S	0.014	0.009	0.607	0.02	0.008	0.007	0.905	0.02
Method (iii) + steam								
B-SiF6-100S-st6	–	–	–	–	0.011	0.009	0.86	0.02

[a] Band area of Brønsted-bonded pyridine at 150 °C referred to the band area of the structural vibration.
[b] Band area of Lewis-bonded pyridine at 150 °C referred to the band area of the structural vibration.

Table 3
Structural properties of $(NH_4)_2SiF_6$-treated materials from N_2 physisorption

	Before use					After use				
	V_{DR}[a] (ml/g)	V_{micro}[b] (ml/g)	V_{meso}[c] (ml/g)	V_{BJH}[d] (ml/g)	LPH[e]	V_{DR}[a] (ml/g)	V_{micro}[b] (ml/g)	V_{meso}[c] (ml/g)	V_{BJH}[d] (ml/g)	LPH[e]
A-550	–	–	–	–	–	0.149	0.151	0.062	0.057	–
Method (i)										
A-SiF6-100aq	0.142	0.146	0.045	0.034	–	0.142	0.143	0.048	0.042	–
Method (ii)										
A-SiF6-100S-aq	0.148	0.139	0.071	0.066	–	0.151	0.152	0.081	0.079	–
Method (iii)										
A-SiF6-20S	0.148	0.150	0.061	0.048	–	0.142	0.142	0.067	0.07	–
A-SiF6-40S	0.139	0.140	0.077	0.069	–	0.139	0.136	0.076	0.077	+
A-SiF6-60S	0.141	0.140	0.073	0.067	+	0.144	0.142	0.080	0.072	+
A-SiF6-100S	0.127	0.128	0.074	0.084	+	0.138	0.136	0.081	0.088	+
Method (iii) + steam										
A-SiF6-100S-st3	–	–	–	–	–	0.139	0.138	0.088	0.086	+
B-550	–	–	–	–	–	0.123	0.128	0.093	0.085	–
Method (iii)										
B-SiF6-100S	0.111	0.110	0.093	0.101	+	0.115	0.114	0.105	0.111	+
Method (iii) + steam										
B-SiF6-100S-st6	–	–	–	–	–	0.12	0.119	0.096	0.098	+

[a] Evaluated according to the method of Dubinin and Raduskevich.
[b] $V(p/p_0 = 0.05)$.
[c] $V_{meso} = V(p/p_0 = 0.99) - V_{micro}$.
[d] Evaluated according to the method of Barrett, Joyner, and Halenda, 22 Å $< d_p <$ 1000 Å.
[e] Existence of low-pressure hysteresis.

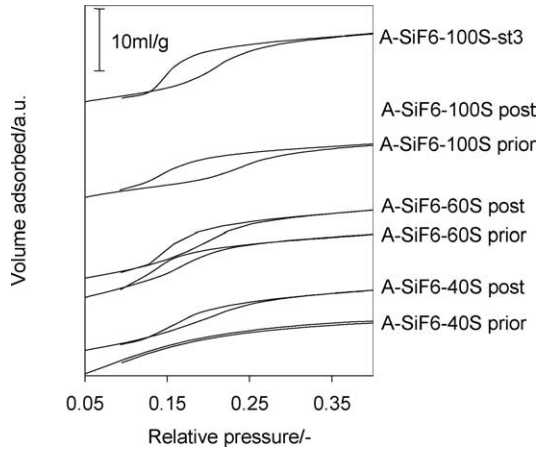

Fig. 8. N_2 physisorption isotherms at 77 K of $(NH_4)_2SiF_6$-treated samples according to method (iii) before and after catalytic testing and steam treatment. Samples derived from basis material A.

work the low-pressure hysteresis was found exclusively for those aluminosilicates treated with $(NH_4)_2SiF_6$ according to method (iii). This is a clear indication that method (iii) is the most efficient method of the three for reducing the FAL content. It must be taken into account that finally 6 mol of F^- per mole SiF_6^{2-} in the form of NH_4F, HF, and SiF_4 is released, to the greatest extent at elevated temperature. Not only is FAL attacked by these compounds and almost quantitatively transferred to octahedral AlF_3, but also the removal of framework silicon in the form of volatile SiF_4 is expected, resulting in a partial destruction of the zeolite framework due to the high density of defect sites. Under reaction/regeneration and hydrothermal conditions those partially damaged zones can further collapse, creating greater mesoporosity (see Table 3) and providing building material to heal out defect sites in less heavily damaged zones. Such processes are well known under hydrothermal conditions (see, e.g., [50,51] and references therein), but are assumed to be even more efficient in the presence of volatile fluorinous reagents, as they can provide higher mobility of silicon species. This and the fact that a substantial part of the unreacted $(NH_4)_2SiF_6$ might be reasonably well distributed in the micropores by solid-state diffusion lead to a only negligible loss of microporosity (Table 3), while most efficiently reducing Brønsted acidity (Table 2). In addition materials with a higher level mesoporosity are obtained compared to, e.g., (hydro)thermally treated materials [52]. With increasing severity of dealumination, i.e., amount of SiF_6^{2-} added, the fraction of aluminum contributing to any kind of acidity ($(A_{Br} + A_{Le})_{spec.}$ in Table 2) decreases; this indicates that a substantial part of the aluminum present in the material is not part of the zeolite, i.e., built into the framework or as EFAL with a high dispersion in the micropores, but in an amorphous phase accessible neither to probe molecules nor to reactants. In some cases a slight increase in Lewis acidity, as a consequence of hydrothermal treatment or after catalytic tests, is observed, above all in the case of deeply dealuminated samples.

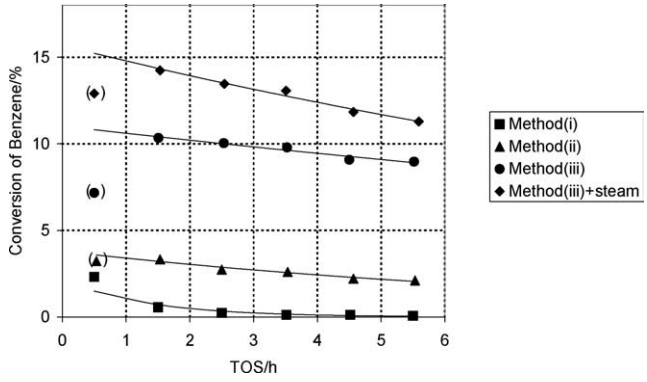

Fig. 9. Conversion of benzene as a function of time on stream (TOS). Reaction conditions: $W/F = 20$ (kg_{cat} s)/mol, $C_6H_6/N_2O/N_2 \approx 4/2/1$ (molar), $S > 95\%$, 425 °C. Parameter: method of preparation. Samples derived from basis material A. Lines are recalculated with Eq. (3). Values in parentheses not taken into account for regression.

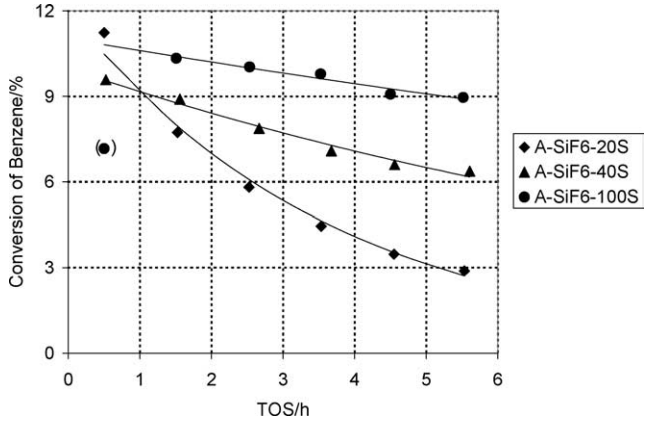

Fig. 10. Conversion of benzene as a function of time on stream (TOS) for samples dealuminated according to method (iii). Parameter: theoretical exchange degree. Reaction conditions: $W/F = 20$ (kg_{cat} s)/mol, $C_6H_6/N_2O/N_2 \approx 4/2/1$ (molar), $S > 95\%$, 425 °C. Samples derived from basis material A. Lines are recalculated with Eq. (3). Values in parentheses not taken into account for regression.

3.2. Catalysis

As outlined above, the elemental composition and physicochemical properties of $(NH_4)_2SiF_6$-treated materials change substantially before and after use. Thus catalytic performance has been checked in regular time scales under certain standard conditions, to ensure that the material does not alter its properties unpredictably during the course of a series of experiments or even during one experiment. Typically the first experiment and the last experiment in a series of five reaction/regeneration cycles were performed under identical reaction conditions. The results of the catalysis were comparable within the experimental error, implying that the modifications take place over a short period of time, possibly during the conditioning of the catalyst or during the first few minutes under reaction conditions.

Activity plots (i.e., conversion of benzene at a constant selectivity as a function of time on stream) are shown in Figs. 9 and 10. Comparing the three different preparation

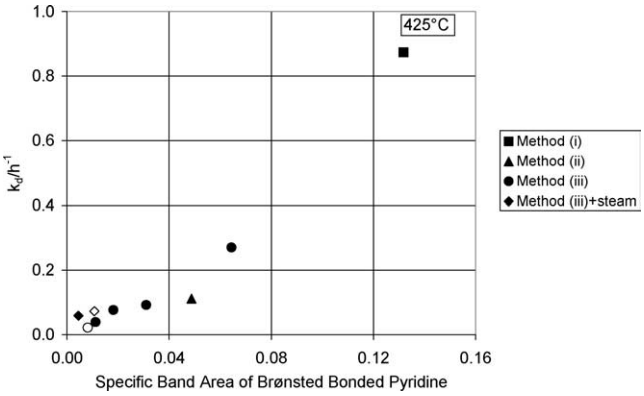

Fig. 11. Rate constant of deactivation k_d as a function of density of Brønsted acid sites. Reaction conditions: $W/F = 20$ (kg_{cat} s)/mol, $C_6H_6/N_2O/N_2 \approx 4/2/1$ (molar), $S > 95\%$, 425 °C. Filled symbols: samples derived from basis material A, open symbols: samples derived from basis material B.

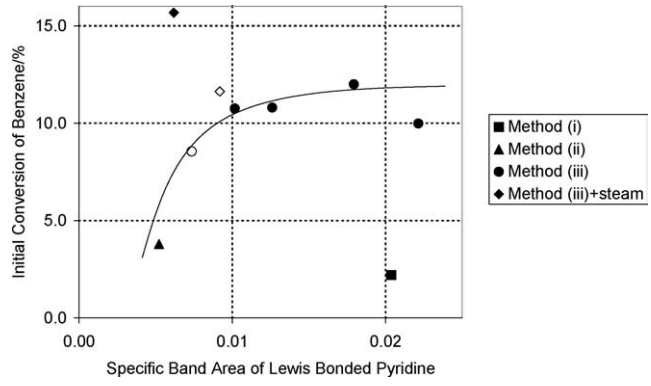

Fig. 12. Initial conversion X_0 of benzene as a function of density of Lewis acid sites. Reaction conditions: $W/F = 20$ (kg_{cat} s)/mol, $C_6H_6/N_2O/N_2 \approx 4/2/1$ (molar), $S > 95\%$, 425 °C. Filled symbols for samples derived from basis material A, empty symbols for samples derived from basis material B.

methods (Fig. 9), it is obvious that method (iii) with a given amount of $(NH_4)_2SiF_6$ (100% theoretical exchange degree) results in the most active catalyst for the reaction under investigation. A significant enhancement of catalytic activity can be achieved by a subsequent steaming procedure. Materials obtained after treatment with method (ii) show moderate activity, whereas materials prepared with the aqueous procedure (method (i)) hardly catalyze the desired reaction. The catalytic performance follows the same trend as the degree of dealumination that can be reached by the different procedures (vide supra).

Fig. 10 shows activity plots for materials prepared according to method (iii) with different theoretical degrees of exchange. Whereas the initial activity is high for all the samples, a clear difference in the rate of deactivation is observed. Obviously the resistance to activity loss is increased with increasing degree of dealumination, i.e., with decreasing density of Brønsted sites as already postulated by Kustov et al. [12] in the case of thermally treated ZSM-5 and by Notté [5] in the case of hydrothermally treated and partially Na-exchanged ZSM-5.

The assumption that bridging hydroxyls play a key role in catalyst deactivation is supported by the correlation shown in Fig. 11. There is a clear trend between the rate constant of deactivation k_d and the density of Brønsted sites, regardless of the basis material and the dealumination method. The initial activity, i.e., the partial pressure of phenol, does not seem to be a decisive factor, since the most active materials (method (iii) and subsequently steamed) show simultaneously high resistance against deactivation.

With respect to catalytic activity a formal correlation between the initial conversion X_0, not yet affected by coking, and the density of Lewis acid sites is established (Fig. 12) regardless of the level of iron impurities. For materials with a comparable mesoporous volume, catalytic activity initially increases with density of Lewis acid sites until a constant level is reached, similar to the correlation found, e.g., by Pirutko et al. [53] for the admixture of iron to various MFI matrices. This is an indication that not only the density of active sites—whether related to Lewis acidic iron or aluminum species—but also their accessibility under reaction conditions are key factors for catalytic activity.

The increase in mesoporous volume due to the dealumination procedure is associated with the creation of a secondary pore system. Therefore, the intracrystalline diffusion path decreases significantly, thus overcoming pore-diffusion limitations. This also explains the outliers in Fig. 12. The surprisingly high activity of the subsequently steam-treated sample A-SiF6-100S-st3 is attributed to the higher degree of mesoporosity and the relatively low activity of sample A-SiF6-100Saq (method (i)) is attributed to the decrease in mesoporosity upon aqueous treatment with $(NH_4)_2SiF_6$ (Table 3). Control of the overall rate by diffusion in the zeolite's micropores has also been observed by Vogel et al. [54] in the case of gas-phase hydroxylation of toluene with N_2O and will be the subject of separate paper including results obtained by the application of other dealumination methods [52].

4. Conclusions

The comparative study of three different methods for framework dealumination with $(NH_4)_2SiF_6$, on the physicochemical properties of the resulting materials before and after reaction and on their catalytic performance for the direct oxidation of benzene, leads to the following conclusions:

- Materials before and after catalytic tests are different; the extent of this difference depends on the initial content of F^-. The modifications seem to take place quickly under reaction conditions.
- Tetrahedrally coordinated aluminum is present in deeply dealuminated materials, though is probably in an amorphous phase.
- Solid-state substitution with subsequent washing in water is more efficient in replacing FAL than the procedure

taking place in the liquid phase. Moreover, mesoporosity is created, improving the catalytic performance of the desired reaction.

- Solid-state substitution with subsequent thermal treatment is the most effective method for elimination of Brønsted acidity and for creating both Lewis acidity and mesoporosity simultaneously.
- Catalytic performance of those materials can be described on the basis of their acid–base and textural properties. The rate of deactivation is governed by the density of Brønsted acidity. Catalytic activity can be related to the density of Lewis acid sites and their accessibility. This observation is supported by the findings of Kustov et al. [12] and Motz et al. [13,14] who regarded Lewis acid FAL and EFAL as active sites for the investigated reaction. The results are also in line with the recent findings of Hensen et al. [11].

References

[1] E. Suzuki, K. Nakashiro, Y. Ono, Chem. Lett. (1988) 953.
[2] M. Gubelmann, P.J. Tirel, US patent 5 001 280 (1991), to Rhone-Poulenc Chimie.
[3] A.S. Kharitanov, G.I. Panov, K.G. Ione, V.N. Romannikov, G.A. Sheveleva, L.A. Vostrikova, V.I. Sobolev, US patent 5 110 995 (1992); to Boreskov Institute of Catalysis.
[4] R. Burch, C. Howitt, Appl. Catal. A 86 (1992) 139.
[5] P. Notté, Top. Catal. 13 (2000) 387.
[6] G.I. Panov, A.K. Uriarte, M.A. Rodkin, V.I. Sobolev, Catal. Today 41 (1998) 365.
[7] G.I. Panov, Cattech 4 (2000) 18.
[8] P. Kubánek, B. Wichterlová, Z. Sobalík, J. Catal. 211 (2002) 109.
[9] D. Meloni, R. Monaci, V. Solinas, G. Berlier, S. Bordiga, I. Rossetti, C. Oliva, L. Forni, J. Catal. 214 (2003) 169.
[10] J. Jia, K.S. Pillai, W.M.H. Sachtler, J. Catal. 221 (2004) 119.
[11] E.J.M. Hensen, Q. Zhu, R.A. van Santen, J. Catal. 220 (2003) 260.
[12] L.M. Kustov, A.L. Tarasov, V.I. Bogdan, A.A. Tyrlov, J.W. Fulmer, Catal. Today 61 (2000) 123.
[13] J.L. Motz, H. Heinichen, W.F. Hölderich, Stud. Surf. Sci. Catal. 105 (1997) 1053.
[14] J.L. Motz, H. Heinichen, W.F. Hölderich, J. Mol. Catal. A: Chem. 136 (1998) 175.
[15] R. Burch, C. Howitt, Appl. Catal. A 106 (1993) 167.
[16] D.P. Ivanov, M.A. Rodkin, K.A. Dubkov, A.S. Kharitanov, G.I. Panov, Kinet. Catal. 41 (2000) 850.
[17] H. Kodama, S. Okazaki, J. Catal. 132 (1991) 512.
[18] N.A. Sánchez, J.M. Saniger, J.-B. d'Espinose de la Caillerie, A.L. Blumenfeld, J.J. Fripiat, Micropor. Mesopor. Mater. 50 (2001) 41.
[19] G.W. Skeels, D.W. Breck, EP patent 82211 A1 19830629 (1983), to Union Carbide Corp.
[20] H.K. Beyer, G. Palné-Borbély, US patent 5 411 724 (1993), to W.R. Grace&Co.
[21] H.K. Beyer, G. Borbély-Pálné, J. Wu, Stud. Surf. Sci. Catal. 84 (1994) 933.
[22] M.M. Dubinin, J. Colloid Interface Sci. 23 (1967) 487.
[23] E.P. Barrett, L.Y. Joyner, P.P. Halenda, J. Chem. Soc., Chem. Commun. 73 (1951) 373.
[24] O. Levenspiel, J. Catal. 25 (1972) 265.
[25] I. Kiricsi, C. Flego, G. Pazzuconi, W.O. Parker Jr., R. Millini, C. Perego, G. Bellussi, J. Phys. Chem. 98 (1994) 4627.
[26] E. Loeffler, C. Peuker, H.G. Jerschkewitz, Catal. Today 3 (1988) 415.
[27] P.A. Jacobs, R. von Ballmoos, J. Phys. Chem. 86 (1982) 3050.
[28] E. Loeffler, U. Lohse, C. Peuker, G. Oehlmann, L.M. Kustov, V.L. Zholobenko, V.B. Kazansky, Zeolites 10 (1990) 266.
[29] M.S. Rigutto, R. de Ruiter, J.P.M. Niederer, H. van Bekkum, Stud. Surf. Sci. Catal. 84 (1994) 2245.
[30] M. Hesse, H. Meier, B. Zeeh, Spektroskopische Methoden in der organischen Chemie, Thieme, Stuttgart, 1995.
[31] R. Le Van Mao, T.S. Le, M. Fairbairn, A. Muntasar, S. Xiao, G. Denes, Appl. Catal. A 185 (1999) 41.
[32] R.B. Borade, A. Clearfield, J. Chem. Soc., Faraday Trans. 91 (1995) 539.
[33] M.C. Cruickshank, L.S. Dentglesser, S.A.I. Barri, J. Chem. Soc., Chem. Commun. (1986) 23.
[34] W.A. Buckermann, C.B. Huong, F. Fajula, Zeolites 13 (1993) 410.
[35] J.P. Gilson, G.C. Edwards, A.W. Peters, K. Rajagopalan, R.F. Wormsbecher, T.G. Roberie, M.P. Shatlock, J. Chem. Soc., Chem. Commun. (1987) 91.
[36] J. Sanz, V. Fornés, A. Corma, J. Chem. Soc., Faraday Trans. 84 (1988) 3113.
[37] E. Brunner, H. Ernst, D. Freude, M. Hunger, C.B. Krause, D. Prager, W. Reschetilowski, W. Schwieger, K.H. Bergk, Zeolites 9 (1989) 282.
[38] D. Freude, M. Hunger, H. Pfeifer, Z. Phys. Chem. NF 152 (1987) 171.
[39] A. Samoson, E. Lipmaa, G. Engelhardt, U. Lohse, H.G. Jerschkewitz, Chem. Phys. Lett. 134 (1987) 589.
[40] J.A. van Bokhoven, A. Kentgens, J.T. Miller, D.C. Koningsberger, in: International Symposium on Acid–Base Catalysis, (Rolduc (NL))O20, 1997.
[41] M. Müller, G. Harvey, R. Prins, Micropor. Mesopor. Mater. 34 (2000) 281.
[42] G.H. Kuehl, H.K.C. Timken, Micropor. Mesopor. Mater. 35–36 (2000) 521.
[43] E. Bourgeat-Lami, P. Massiani, F. Di Renzo, F. Fajula, T. Des Courieres, Catal. Lett. 5 (1990) 265.
[44] E. Bourgeat-Lami, P. Massiani, F. Di Renzo, F. Fajula, Appl. Catal. 72 (1991) 139.
[45] S. Han, K. Schmitt, S.E. Schramm, D.S. Shihabi, C.D. Chang, Inorg. Chim. Acta 229 (1995) 81.
[46] U. Mueller, K.K. Unger, Stud. Surf. Sci. Catal. 39 (1987) 101.
[47] K.S.W. Sing, D.H. Everett, R.A.W. Haul, L. Moscou, R.A. Pierotti, J. Rouquerol, T. Siemieniewska, Pure Appl. Chem. 57 (1985) 603.
[48] P.L. Llewellyn, J.-P. Coulomb, Y. Grillet, J. Patarin, H. Lauter, H. Reichert, J. Rouquerol, Langmuir 9 (1993) 1846.
[49] P.L. Llewellyn, J.-P. Coulomb, Y. Grillet, J. Patarin, G. Andre, J. Rouquerol, Langmuir 9 (1993) 1852.
[50] J.A. Martens, W. Souverijns, W. van Rhijn, P.A. Jacobs, in: G. Ertl, H. Knözinger, J. Weitkamp (Eds.), Handbook of Heterogeneous Catalysis, vol. 1, VCH–Wiley, Weinheim, 1997, p. 325.
[51] G. Kuehl, in: J. Weitkamp, L. Puppe (Eds.), Catalysis and Zeolites—Fundamentals and Applications, Springer, Berlin, 1999, p. 81.
[52] F. Kollmer, H. Hausmann, W.F. Hölderich, J. Catal., accepted.
[53] L.V. Pirutko, V.S. Chernyavsky, A.K. Uriarte, G.I. Panov, Appl. Catal. A 227 (2002) 143.
[54] B. Vogel, C. Schneider, E. Klemm, Catal. Lett. 79 (2002) 107.